Available online at www.sciencedirect.com
SCIENCE DIRECT®
Journal of Sound and Vibration 277 (2004) 31–48
JOURNAL OF SOUND AND VIBRATION
www.elsevier.com/locate/jsvi

Limit cycles, bifurcations, and accuracy of the milling process

B.P. Mann[a,*], P.V. Bayly[b], M.A. Davies[c], J.E. Halley[d]

[a] *Department of Mechanical and Aerospace Engineering, University of Florida, P.O. Box 116300, Gainesville, FL 32611, USA*
[b] *Department of Mechanical Engineering, Washington University, St. Louis, MO, USA*
[c] *Department of Mechanical Engineering, University of North Carolina, Charlotte, NC, USA*
[d] *Tech Manufacturing, Wright City, MO, USA*

Received 14 October 2002; accepted 19 August 2003

Abstract

Time finite element analysis (TFEA) is used to determine the accuracy, stability, and limit cycle behavior of the milling process. Predictions are compared to traditional Euler simulation and experiments. The TFEA method forms an approximate solution by dividing the time in the cut into a finite number of elements. The approximate solution is then matched with the exact solution for free vibration to obtain a discrete linear map. Stability is then determined from the characteristic multipliers of the map. Map fixed points correspond to stable periodic solutions which are used to evaluate surface location error. Bifurcations and limit cycle behavior are predicted from a non-linear TFEA formulation. Experimental cutting tests are used to confirm theoretical predictions.
© 2003 Elsevier Ltd. All rights reserved.

1. Introduction

Relative vibrations between a cutting tool and workpiece result in a machining process with surface location errors and time-varying chip loads. Since cutting forces are approximately proportional to the uncut chip area [1–4], chip load variations cause dynamic cutting forces which may excite the structural modes of a machine–tool system resulting in unstable vibrations known as *chatter*. Unless avoided, chatter vibrations may cause large dynamic loads on the machine spindle and table structure, damage to the cutting tool, and a poor surface finish [1,5]. Therefore, it is desirable to avoid chatter vibrations. Even in the absence of chatter, the accurate placement of a machined surface is complicated by vibrations and surface location errors result when the machined surface does not lie "exactly" at the commanded location.

*Corresponding author. Tel.: +1-352-392-4550; fax: +1-352-392-1071.
E-mail address: bmann@ufl.edu (B.P. Mann).

0022-460X/$ - see front matter © 2003 Elsevier Ltd. All rights reserved.
doi:10.1016/j.jsv.2003.08.040

The explanation for machine–tool chatter was first given by Tlusty [6] and Tobias [7] as "regeneration of waviness". The resulting mathematical equations are in the form of delay-differential equations. Stability predictions have been made in the case of continuous cutting by several authors [1,7,8]. These solutions are only approximate for the case of milling because the direction of the cutting force changes with tool rotation and cutting is interrupted as each tooth enters and leaves the workpiece (see Fig. 1). While numerical simulation can be used to capture the interrupted nature of the milling process (see Ref. [9]), the exploration of parameter space by time domain simulation is inefficient. The desire for a more efficient analytical method has led to development of several alternative methods for the prediction of stability properties in milling, e.g., Refs. [10–13].

Analytical investigations have predicted the occurrence of new bifurcation phenomena in interrupted cutting processes. In addition to Hopf bifurcations, period doubling bifurcations have been analytically predicted by Davies et al. [11], Insperger and Stépán [14], Corpus and Endres [15], Bayly et al. [16] and confirmed experimentally by Davies et al. [11], Bayly et al. [16], and Mann et al. [17].

In this paper, a new approach is described to predict stability, surface location error, and the limit cycle behavior in milling. The solution technique, called time finite element analysis or (TFEA), forms an approximate solution by dividing the time in the cut into a finite number of elements. The approximate solution is then matched with the exact solution for free vibration to obtain a discrete linear map. The characteristic multipliers or eigenvalues of the map are used to determine the stability of the system. Fixed points of the dynamic map are used to predict the steady state surface location errors in stable cutting processes that result from tool or workpiece vibrations.

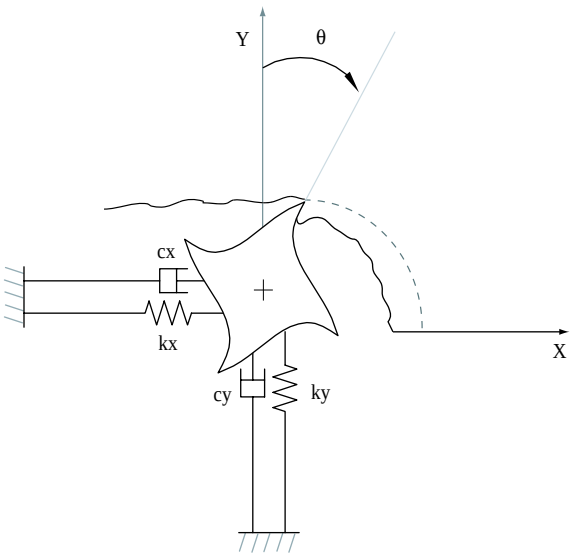

Fig. 1. Two-degree-of-freedom milling process. A single mode in each direction is considered. Equations are analogous if the tool is assumed rigid and the workpiece is flexible.

For an unstable cutting process, relative vibrations build until the tool jumps out of the cut. When the tool continues to reenter and jump out of the cut, the result is a limit cycle. A recursive mapping process, called non-linear TFEA, is introduced here to capture the non-linearity of the tool jumping out of the cut.

The stability, accuracy, and limit cycle predictions from the TFEA method are compared to experimental cutting tests and Euler simulation. Strong agreement is obtained between the both numerical methods and experiments. In addition, the computation times required for TFEA predictions is shown to be significantly less than computational times for Euler simulation.

2. Mechanical model

A schematic diagram of a two-degree-of-freedom milling process is shown in Fig. 1. A compliant tool or structure with a single mode of vibration in two uncoupled and orthogonal directions will result in the following equation of motion:

$$\begin{bmatrix} m_x & 0 \\ 0 & m_y \end{bmatrix} \begin{bmatrix} \ddot{x}(t) \\ \ddot{y}(t) \end{bmatrix} + \begin{bmatrix} c_x & 0 \\ 0 & c_y \end{bmatrix} \begin{bmatrix} \dot{x}(t) \\ \dot{y}(t) \end{bmatrix} + \begin{bmatrix} k_x & 0 \\ 0 & k_y \end{bmatrix} \begin{bmatrix} x(t) \\ y(t) \end{bmatrix} = \begin{bmatrix} F_x(t) \\ F_y(t) \end{bmatrix}, \tag{1}$$

where the terms $m_{x,y}$, $c_{x,y}$, $k_{x,y}$, and $F_{x,y}$ are the modal mass, damping, spring stiffness, and cutting forces in the flexible directions of the system. The x and y cutting force components on the pth tooth are given by

$$F_{xp}(t) = -g_p(t)[F_{tp}(t)\cos\theta_p(t) + F_{np}(t)\sin\theta_p(t)], \tag{2}$$

$$F_{yp}(t) = g_p(t)[F_{tp}(t)\sin\theta_p(t) - F_{np}(t)\cos\theta_p(t)], \tag{3}$$

where $g_p(t)$ acts as a switching function, it is equal to one if the pth tooth is active and zero if it is not cutting [10,12]. The tangential and normal cutting force components, $F_{tp}(t)$ and $F_{np}(t)$, respectively, are considered to be the product of linearized cutting coefficients K_t and K_n, the nominal depth of cut b, and the instantaneous chip width $w_p(t)$:

$$F_{tp}(t) = K_t b w_p(t), \;\; F_{np}(t) = K_n b w_p(t), \tag{4, 5}$$

where $w_p(t)$ depends upon the feed per tooth, h, the cutter rotation angle $\theta_p(t)$, and regeneration in the compliant structure directions:

$$w_p(t) = h\sin\theta_p(t) + [x(t) - x(t-\tau)]\sin\theta_p(t) + [y(t) - y(t-\tau)]\cos\theta_p(t). \tag{6}$$

Here, $h\sin\theta_p(t)$ is the circular tool path approximation [1,5], $\tau = 60/N\Omega$ [s] is the tooth pass period, Ω is the spindle speed given in r.p.m. and N is the total number of cutting teeth. The angular position of the pth tooth for a cutter with evenly spaced teeth is $\theta_p(t) = (2\pi\Omega/60)t + p2\pi/N$.

The total cutting force equations are found by summing the forces on each cutting tooth and substituting Eqs. (4)–(6) into Eqs. (2) and (3):

$$\begin{bmatrix} F_x \\ F_y \end{bmatrix} = \sum_{p=1}^{N} g_p(t) b \left(h \begin{bmatrix} -K_t sc - K_n s^2 \\ K_t s^2 - K_n sc \end{bmatrix} + \begin{bmatrix} -K_t sc - K_n s^2 & -K_t c^2 - K_n sc \\ K_t s^2 - K_n sc & K_t sc - K_n c^2 \end{bmatrix} \begin{bmatrix} x(t) - x(t-\tau) \\ y(t) - y(t-\tau) \end{bmatrix} \right), \tag{7}$$

where $s = \sin\theta_p(t)$ and $c = \cos\theta_p(t)$. A more compact form for the equation of motion and is realized by defining the substitutions

$$\mathbf{K}_c(t) = \sum_{p=1}^{N} g_p(t) \begin{bmatrix} -K_t sc - K_n s^2 & -K_t c^2 - K_n sc \\ K_t s^2 - K_n sc & K_t sc - K_n c^2 \end{bmatrix}, \tag{8}$$

$$\boldsymbol{f}_0(t) = \sum_{p=1}^{N} g_p(t) h \begin{bmatrix} -K_t sc - K_n s^2 \\ K_t s^2 - K_n sc \end{bmatrix}, \tag{9}$$

and rewriting Eq. (1) as

$$\mathbf{M}\ddot{\boldsymbol{X}}(t) + \mathbf{C}\dot{\boldsymbol{X}}(t) + \mathbf{K}\boldsymbol{X}(t) = \mathbf{K}_c(t) b[\boldsymbol{X}(t) - \boldsymbol{X}(t-\tau)] + \boldsymbol{f}_0(t) b, \tag{10}$$

where $\boldsymbol{X}(t) = [x(t)\ y(t)]^{\top}$ is the two-element position vector and $\mathbf{M}, \mathbf{C}$, and $\mathbf{K}$ are the 2×2 mass, damping, and stiffness matrices of Eq. (1). When the structure is only compliant in a single direction, Eq. (10) can be modified by eliminating the corresponding rows and columns of the opposing direction. For instance, a structure compliant only in the x direction would have the following equation of motion:

$$m_x \ddot{x}(t) + c_x \dot{x}(t) + k_x x(t) = -K_{sx}(t) b[x(t) - x(t-\tau)] - f_{0x}(t) b, \tag{11}$$

where the x direction terms of $\mathbf{K}_c(\theta(t))$ and $\boldsymbol{f}_0(\theta(t))$ have now been written as

$$K_{sx}(t) = \sum_{p=1}^{N} g_p(t)[K_t \cos\theta_p(t) + K_n \sin\theta_p(t)]\sin\theta_p(t), \tag{12}$$

$$f_{0x}(t) = \sum_{p=1}^{N} g_p(t)[K_t \cos\theta_p(t) + K_n \sin\theta_p(t)] h \sin\theta_p(t). \tag{13}$$

The terms $K_{sx}(t)$ and $f_{0x}(t)$ provide a periodic forcing term which would result in a periodic solution in the absence of the perturbations given by the time-delayed relative displacement terms of Eq. (11). Perturbation growth reflects the loss of stability, while perturbation decay characterizes an asymptotically stable cutting process.

3. TFEA

The dynamic behavior of the milling process is dependent upon a time-delay differential equation which does not have a closed form solution. Therefore, an approximate solution is

sought to understand the behavior of the system. One such approximation technique used for dynamic systems is TFEA [18]. This method was first applied to an interrupted turning process by Halley [19] and Bayly et al. [20]. The authors matched an approximation for the cutting motion obtained using a single finite element to the exact solution for free vibration to obtain a discrete linear map. The characteristic multipliers or eigenvalues of the map were used to determine the stability of the system. Comparisons with experimental tests showed strong agreement for small fractions of the spindle period in the cut (ρ). However, diminished correlations were shown for larger values of ρ. This was corrected in Bayly et al. [16] by dividing the time in the cut into multiple finite elements in time. The multiple element turning solution was adapted to model single-degree-of-freedom (SDOF) milling systems in Mann et al. [17] and multiple degree of freedom systems (MDOF) in Bayly et al. [21]. The analysis presented in this article extends the previous stability SDOF work of Mann et al. [17] to the prediction of surface location error and the limit cycle behavior associated with the non-linearity of the tool exiting the cut during chatter vibrations. The formulation of the dynamic map for the MDOF system (Eq. (10)) closely follows the discretization procedure outlined in Bayly et al. [21], but has been presented here for completeness.

3.1. Free vibration

When the tool is not in contact with the workpiece, the system is governed by the equation for free vibration

$$\mathbf{M}\ddot{\boldsymbol{X}}(t) + \mathbf{C}\dot{\boldsymbol{X}}(t) + \mathbf{K}\boldsymbol{X}(t) = 0. \tag{14}$$

This equation can be rearranged into state-space form

$$\begin{bmatrix} \dot{\boldsymbol{X}}(t) \\ \ddot{\boldsymbol{X}}(t) \end{bmatrix} = \begin{bmatrix} 0 & I \\ -\mathbf{M}^{-1}\mathbf{K} & -\mathbf{M}^{-1}\mathbf{C} \end{bmatrix} \begin{bmatrix} \boldsymbol{X}(t) \\ \dot{\boldsymbol{X}}(t) \end{bmatrix}, \tag{15}$$

where the 2×2 state matrix in Eq. (15) will be denoted by $\mathbf{G}$. If we let $t = t_c$ as the tool leaves the material and t_f be the duration of free vibration, a state transition matrix ($\mathbf{\Phi} = e^{\mathbf{G}t_f}$) can be obtained that relates the state of the tool at the beginning of free vibration to the state of the tool at the end of free vibrations.

This equation is true for every period, such that for all n:

$$\begin{bmatrix} \boldsymbol{X}(n\tau) \\ \dot{\boldsymbol{X}}(n\tau) \end{bmatrix} = \mathbf{\Phi} \begin{bmatrix} \boldsymbol{X}((n-1)\tau + t_c) \\ \dot{\boldsymbol{X}}((n-1)\tau + t_c) \end{bmatrix}. \tag{16}$$

3.2. Vibration during cutting

When the tool is in the cut, its motion is governed by a time-delayed differential equation. Since this equation does not have a closed form solution, an approximate solution for the tool displacement is assumed for the jth element of the nth tooth passage as a linear combination of

polynomials (see Ref. [22])

$$\boldsymbol{X}(t) = \sum_{i=1}^{4} \boldsymbol{a}_{ji}^{n} \phi_i(\sigma_j(t)). \tag{17}$$

Here, $\sigma_j(t) = t - n\tau - \sum_{k=1}^{j-1} t_k$ is the "local" time within the jth element of the nth period, the length of the kth element is t_k and the trial functions $\phi_i(\sigma_j(t))$ are the cubic Hermite polynomials. On the jth element these functions are

$$\phi_1(\sigma_j) = 1 - 3\left(\frac{\sigma_j}{t_j}\right)^2 + 2\left(\frac{\sigma_j}{t_j}\right)^3, \tag{18a}$$

$$\phi_2(\sigma_j) = t_j\left[\left(\frac{\sigma_j}{t_j}\right) - 2\left(\frac{\sigma_j}{t_j}\right)^2 + \left(\frac{\sigma_j}{t_j}\right)^3\right], \tag{18b}$$

$$\phi_3(\sigma_j) = 3\left(\frac{\sigma_j}{t_j}\right)^2 - 2\left(\frac{\sigma_j}{t_j}\right)^3, \tag{18c}$$

$$\phi_4(\sigma_j) = t_j\left[-\left(\frac{\sigma_j}{t_j}\right)^2 + \left(\frac{\sigma_j}{t_j}\right)^3\right]. \tag{18d}$$

These functions are particularly useful because they allow the coefficients of the assumed solution to be found by matching the initial and final velocities for each element.

Substitution of the assumed solution (Eq. (17)) into the equation of motion (Eq. (11)) leads to a non-zero error. The error from the assumed solution is "weighted" by multiplying by a set of test functions and setting the integral of the weighted error to zero to obtain two equations per element [16,19,20,22,23]. The test functions are chosen to be the simplest possible functions: $\psi_1(\sigma_j) = 1$ (constant) and $\psi_2(\sigma_j) = \sigma_j/t_j - 1/2$ (linear). The integral is taken over the time for each element, $t_j = t_c/E$, thereby dividing the time in the cut t_c into E elements. The resulting two equations are

$$\begin{aligned}\int_0^{t_j} \Bigg[& \mathbf{M}\left(\sum_{i=1}^{4} \boldsymbol{a}_{ji}^{n} \ddot{\phi}_i(\sigma_j)\psi_p(\sigma_j)\right) + \mathbf{C}\left(\sum_{i=1}^{4} \boldsymbol{a}_{ji}^{n} \dot{\phi}_i(\sigma_j)\psi_p(\sigma_j)\right) \\ & + (\mathbf{K} - b\mathbf{K}_c(\sigma_j))\left(\sum_{i=1}^{4} \boldsymbol{a}_{ji}^{n} \phi_i(\sigma_j)\psi_p(\sigma_j)\right) \\ & + bK_c(\sigma_j)\left(\sum_{i=1}^{4} \boldsymbol{a}_{ji}^{n-1} \phi_i(\sigma_j)\psi_p(\sigma_j)\right) - b\boldsymbol{f}_0(\sigma_j)\psi_p(\sigma_j)\Bigg] \mathrm{d}\sigma_j = 0, \quad p = 1, 2.\end{aligned} \tag{19}$$

Here p is used to identify the test function and the terms $\mathbf{K}_c(\sigma_j)$ and $\boldsymbol{f}_0(\sigma_j)$ have been used in place of the previously defined $\mathbf{K}_c(t)$ and $\boldsymbol{f}_0(t)$ to explicitly show dependence on the local time.

The displacement and velocity at tool entry into the cut are specified by the coefficients of the first two basis functions on the first element: $\boldsymbol{a}_{11}^{n}$ and $\boldsymbol{a}_{12}^{n}$. The relationship between the initial and final conditions during free vibration can be rewritten in terms of the

coefficients as

$$\begin{pmatrix} \boldsymbol{a}_{11} \\ \boldsymbol{a}_{12} \end{pmatrix}^n = \boldsymbol{\Phi} \begin{pmatrix} \boldsymbol{a}_{E3} \\ \boldsymbol{a}_{E4} \end{pmatrix}^{n-1}, \tag{20}$$

where E is the total number of finite elements in the cut. For the remainder of the elements, a continuity constraint is imposed to set the position and velocity at the end of one element are equal to the position and velocity at the beginning of the next element.

Eqs. (19) and (20) can be arranged into a global matrix relating the coefficients of the assumed solution in terms of the coefficients of the previous tooth passage. The following expression is for the case when the number of elements is $E = 3$:

$$\begin{bmatrix} \mathbf{I} & \mathbf{0} & \mathbf{0} & \mathbf{0} \\ \mathbf{N}_1^1 & \mathbf{N}_2^1 & \mathbf{0} & \mathbf{0} \\ \mathbf{0} & \mathbf{N}_1^2 & \mathbf{N}_2^2 & \mathbf{0} \\ \mathbf{0} & \mathbf{0} & \mathbf{N}_1^3 & \mathbf{N}_2^3 \end{bmatrix} \begin{bmatrix} \boldsymbol{a}_{11} \\ \boldsymbol{a}_{12} \\ \boldsymbol{a}_{21} \\ \boldsymbol{a}_{22} \\ \boldsymbol{a}_{31} \\ \boldsymbol{a}_{32} \\ \boldsymbol{a}_{33} \\ \boldsymbol{a}_{34} \end{bmatrix}^n = \begin{bmatrix} \mathbf{0} & \mathbf{0} & \mathbf{0} & \Phi \\ \mathbf{P}_1^1 & \mathbf{P}_2^1 & \mathbf{0} & \mathbf{0} \\ \mathbf{0} & \mathbf{P}_1^2 & \mathbf{P}_2^2 & \mathbf{0} \\ \mathbf{0} & \mathbf{0} & \mathbf{P}_1^3 & \mathbf{P}_2^3 \end{bmatrix} \begin{bmatrix} \boldsymbol{a}_{11} \\ \boldsymbol{a}_{12} \\ \boldsymbol{a}_{21} \\ \boldsymbol{a}_{22} \\ \boldsymbol{a}_{31} \\ \boldsymbol{a}_{32} \\ \boldsymbol{a}_{33} \\ \boldsymbol{a}_{34} \end{bmatrix}^{n-1} + \begin{bmatrix} \mathbf{0} \\ \mathbf{0} \\ \boldsymbol{C}_1 \\ \boldsymbol{C}_2 \\ \boldsymbol{C}_1 \\ \boldsymbol{C}_2 \\ \boldsymbol{C}_1 \\ \boldsymbol{C}_2 \end{bmatrix}, \tag{21}$$

where the sub-matrices and elements of the sub-matrices for the jth element are

$$\boldsymbol{N}_1^j = \begin{bmatrix} N_{11}^j & N_{12}^j \\ N_{21}^j & N_{22}^j \end{bmatrix}, \quad \boldsymbol{N}_2^j = \begin{bmatrix} N_{13}^j & N_{14}^j \\ N_{23}^j & N_{24}^j \end{bmatrix}, \tag{22}$$

$$\mathbf{P}_1^j = \begin{bmatrix} P_{11}^j & P_{12}^j \\ P_{21}^j & P_{22}^j \end{bmatrix}, \quad \mathbf{P}_2^j = \begin{bmatrix} P_{13}^j & P_{14}^j \\ P_{23}^j & P_{24}^j \end{bmatrix}, \tag{23}$$

$$N_{pi}^j = \int_0^{t_j} [\mathbf{M}\ddot{\phi}_i(\sigma_j) + \mathbf{C}\dot{\phi}_i(\sigma_j) + (\mathbf{K} - b\mathbf{K}_c(\sigma_j))\phi_i(\sigma_j)]\psi_p(\sigma_j)\,\mathrm{d}\sigma_j, \tag{24}$$

$$P_{pi}^j = \int_0^{t_j} b\mathbf{K}_c(\sigma_j)\phi_i(\sigma_j)\psi_p(\sigma_j)\,\mathrm{d}\sigma_j, \tag{25}$$

$$C_p^j = \int_0^{t_j} b\boldsymbol{f}_0(\sigma_j)\psi_p\,\mathrm{d}\sigma_j. \tag{26}$$

Eq. (21) describes a discrete dynamical system, or map, that can be written as

$$\mathbf{A}\boldsymbol{a}_n = \mathbf{B}\boldsymbol{a}_{n-1} + \boldsymbol{C}, \tag{27}$$

or

$$\boldsymbol{a}_n = \mathbf{Q}\boldsymbol{a}_{n-1} + \boldsymbol{D}. \tag{28}$$

3.3. Stability prediction from dynamic map characteristic multipliers

The eigenvalues of the transition matrix $\mathbf{Q} = \mathbf{A}^{-1}\mathbf{B}$ are called characteristic multipliers (CMs) and take on a discrete mapping analogy to the characteristic exponents that govern stability for continuous systems (see Ref. [24]). The condition for stability is that the magnitudes of the CMs must be in a modulus of less than one for a given spindle speed (Ω) and depth of cut (b) for the milling process to be asymptotically stable. Fig. 2 shows the boundaries between stable and unstable cutting as a function of spindle speed and depth of cut. Two distinct types of instability are illustrated by CM trajectories in the complex plane: (1) a flip bifurcation or period doubling phenomena occurs when a negative real CM passes through the unit circle; (2) a Hopf bifurcation occurs when a complex CM obtains a magnitude greater than one. These routes to instability are illustrated in the bottom graphs of Fig. 2 with the corresponding speed and depth of cut points shown in the top stability chart.

Since TFEA is a numerical technique for approximating the dynamic behavior of a system, it is important to consider the numerical solution convergence. A thorough discussion of various

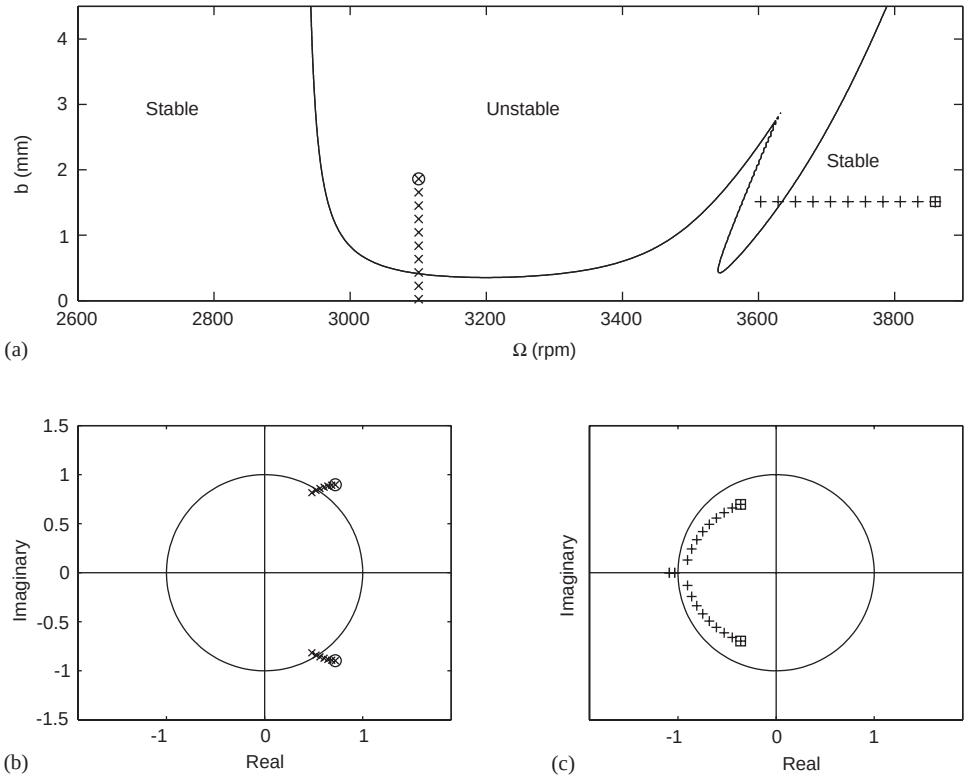

Fig. 2. Stability predictions are made from characteristic multiplier magnitudes; an unstable parameter combination will penetrate the unit circle in the complex plane: (a) up-milling stability predictions; and (b) characteristic multiplier trajectories for a Hopf bifurcation ($\Omega = 3101$ r.p.m., $b = 0$–1.9 mm); and (c) characteristic multiplier trajectories for a flip bifurcation ($\Omega = 3603$–3874 r.p.m., $b = 1.5$ mm). Structure assumed compliant only in the x direction with dynamic and cutting coefficient parameters from Table 1. Computational time of 3.5 min with $E = 3$.

problem formulations, choice of trial functions, and numerical convergence was demonstrated in Peters et al. [22,25]. Bayly et al. [16] demonstrated convergence for interrupted cutting by simply increasing the number of temporal finite elements until stability boundaries no longer changed. For the figures presented in this article, the solution convergence was checked and the number of elements (E) will be included in the figure captions.

3.4. Surface location error from map fixed points

A surface location error results when the machined surface does not lie "exactly" at the commanded location. Several sources of error such as tool or workpiece vibrations, imperfect spindle motions, thermal errors, controller errors, and friction in the machine drives all contribute to the total error [1,4]. The goal of this section is to present a prediction method for the contribution of tool or workpiece vibrations to steady state error. This is achieved by formulating a solution that accounts for changing process parameters such as spindle speed and depth of cut to illustrate their effects on the surface location error.

The TFEA method discretizes the continuous system equations to form the dynamic map shown in Eq. (28). The coefficient vector $\boldsymbol{a}_n$ identifies the velocity and displacement at the beginning and end of each element. Surface location error is given by the displacement coefficient value when the cutting tooth is normal to the surface. This occurs at cutter tooth entry into the cut for up-milling and cutter exit for down-milling.

Stable milling processes have periodic cutting forces and periodic solutions. The steady state coefficients are found from the fixed points ($\boldsymbol{a}_n^*$) of the dynamic map:

$$\boldsymbol{a}_n = \boldsymbol{a}_{n-1} = \boldsymbol{a}_n^*. \tag{29}$$

Substitution of Eq. (29) into Eq. (28) gives the fixed point map solution or steady state coefficient vector

$$\boldsymbol{a}_n^* = (\mathbf{I} - \mathbf{Q})^{-1}\boldsymbol{D}. \tag{30}$$

Since $\mathbf{Q}$ and $\boldsymbol{D}$ can be computed exactly for each spindle speed and depth of cut, the fixed point displacement solution can be found and used to specify surface location error as a function of machining process parameters.

3.5. Non-linear TFEA for limit cycle prediction

Unstable cutting processes produce large cutting forces as relative vibrations between the cutting tool and workpiece build. Both cutting forces and vibrations continue to grow until the tool jumps out of the cut. As the tool jumps out of the cut, the cutting forces become zero and free vibrations occur until the tool reenters the cut. This leads to a limit cycle when the tool continues to re-enter and jump out of the cut. Since the non-linearity associated with the tool jumping out of the cut is not accounted for in the fixed point solution, a modified solution method called non-linear TFEA is presented in this section to predict the milling process limit cycle behavior. This highlights the important aspect that surface location error predictions should only be used for stable cutting processes.

The non-linear TFEA procedure iterates the dynamic map (Eq. (28)) to obtain the current coefficient vector ($\boldsymbol{a}_n$) from the previous tooth passage coefficients ($\boldsymbol{a}_{n-1}$). During each tooth passage, the radial chip width (w_p) is checked at the beginning and end of each element with Eq. (6), where $\boldsymbol{X}(t)$ is equal to the displacement coefficients of $\boldsymbol{a}_n$. If a negative w_p occurs in the jth element, the tool has jumped out of the cut. The cutting forces are then set to zero by changing $\mathbf{K}_c(\sigma_j)$ and $\boldsymbol{f}_0(\sigma_j)$ to zero in Eqs. (24)–(26) and updating the rows of the global matrix (Eq. (21)) corresponding to the $j+1$ element. In addition, the effect of the tool jumping out of the cut is captured in the following revolution by correcting the feed in Eq. (26) to form a new $\boldsymbol{D}$.

4. Euler simulation

A simple Euler time marching scheme is introduced here for comparison purposes with the TFEA method. Euler simulation was chosen because it is a simple, but proven method for simulating the behavior of the milling process [1,4,9,26]. Here the non-linearity encountered during chatter vibrations is incorporated by setting the cutting forces to zero as the tool jumps out of the cut and adjusting the radial chip width in the following tooth passage [1,26,27]. Since direct stability predictions from the Euler simulation equations is not possible, a method for quantifying an unstable cutting process must be adopted to analyze the results of the time marching algorithm. One such alternative is to analyze the statistical variance (σ^2) of the 1/tooth displacements (x_n) as discussed by Schmitz [28,29]

$$\sigma^2 = \frac{\sum_{n=1}^{S}(x_n - \bar{x}_n)^2}{S-1}, \tag{31}$$

where $\bar{x}_n = \sum_{n=1}^{S} x_n/S$ and S is the number of 1/tooth displacement samples. Stability predictions using this method are shown in Fig. 3. The variance was taken over the last 30 of a total of 150 simulated cutter revolutions. The distinction between a stable and unstable cutting process is illustrated by a sharp increase in the variance as shown in the bottom graphs of Fig. 3 with the corresponding speed and depth of cut points shown in the top stability diagram. The variance corresponding to the loss of stability was estimated to be $\sigma^2 = 1 \times 10^{-6}$ (mm^2). The computational time to obtain the Euler simulation results of Fig. 3 was 400 times the TFEA computational time for Fig. 2.

5. Comparison of numerical predictions

A fundamental concept used to characterize the behavior of a system is phase space [24,30,31]. The stroboscopic sampling of phase space, commonly called a Poincaré section or map, can also be used to characterize the behavior of a periodically forced system [24]. Therefore, Poincaré sections have been constructed for the results given in this section using 1/tooth displacement (x_n) and delayed 1/tooth displacement (x_{n2}) co-ordinates.

Iteration of the dynamic map (Eq. (28)) was used to obtain the linear TFEA 1/tooth displacements (x_n) and delayed 1/tooth displacements (x_{n2}) predictions of Fig. 4. The 1/tooth displacements were taken from the coefficient vector $\boldsymbol{a}_n$ at each cutter entry into the cut for

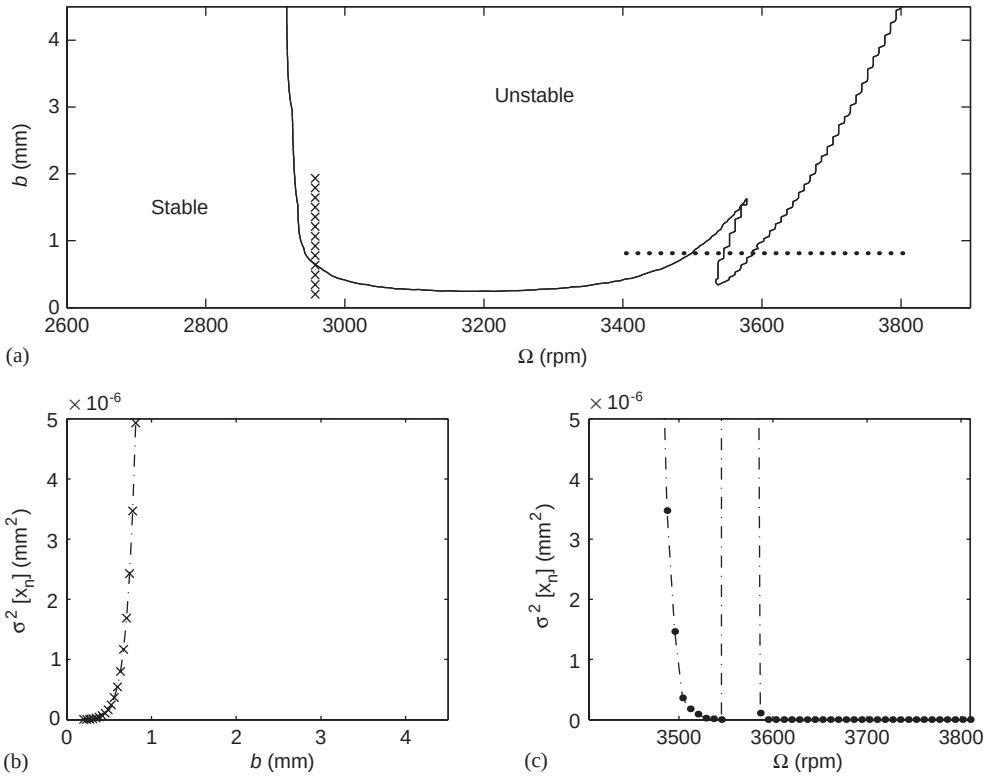

Fig. 3. Euler simulation stability predictions from variance of 1/tooth displacements: (a) simulation stability boundaries with $\sigma^2_{lim} = 1 \times 10^{-6}$ mm^2; (b) variance plot of transition between stable and unstable cutting ($\Omega =$ 2957 r.p.m., $b = 0$–2 mm); and (c) variance plot of transition between stable and unstable cutting ($\Omega =$ 3400–3800 r.p.m., $b = 0.8$ mm). Structure assumed compliant only in the x direction with dynamic and cutting coefficient parameters from Table 1. Computational time of 23.5 h using 400 steps/τ.

up-milling and for each cutter exit for down-milling. In comparison to the Euler simulation predictions of Fig. 5, it is evident that linear TFEA correctly predicts an unstable cutting processes, but it is unable to capture the limit cycle behavior during chatter vibrations.

Predictions using the non-linear TFEA method are shown in Fig. 6. A period doubling or flip bifurcation is predicted in case A of Figs. 5 and 6. Cases B and C predict unstable Hopf bifurcations and capture the limit cycle behavior. A stable cutting process with substantial surface location error is shown by case D of Figs. 4–6. Although the results shown in this section illustrate the most inefficient way to use TFEA, the computational times are still shorter than those made with Euler simulation.

6. Experimental verification

Milling tests were performed using experimental flexures designed to be compliant in a single direction. Each monolithic, uni-directional flexure was machined from aluminum and instrumented with a single non-contact, eddy current displacement transducer as shown in Fig. 7.

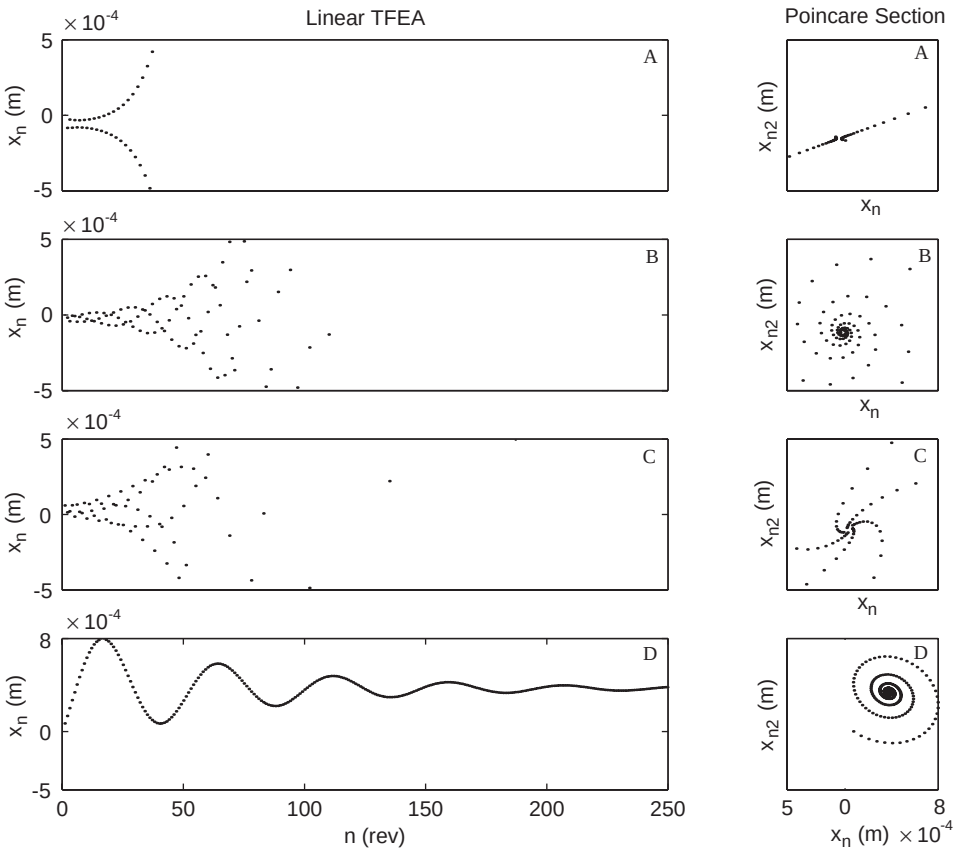

Fig. 4. Predictions of 1/tooth displacements by linear TFEA for cases (A, B, C, D) of Fig. 8. Each row contains a 1/tooth displacement plot and a Poincaré section shown in delayed coordinates. Cases A ($\Omega = 3650$ r.p.m., $b = 2.3$ mm) and B ($\Omega = 3300$ r.p.m., $b = 0.8$ mm) are up-milling examples of flip and Hopf bifurcations, respectively. Cases C ($\Omega = 3600$ r.p.m., $b = 2.1$ mm) and D ($\Omega = 4350$ r.p.m., $b = 3.0$ mm) are down-milling predictions for an unstable Hopf bifurcation and a stable cutting process with substantial surface location error. Structure assumed compliant only in x direction with dynamic and cutting coefficient parameters from Table 1. Computational time of 15 s/case using $E = 25$.

The modal mass, damping, and stiffness parameters were determined using the methods outlined by Refs. [17,32] and are shown in Table 1. In comparison to the compliant direction of each flexure, the values of stiffness in the perpendicular directions were more than 20 times greater, as was the stiffness of the tool. The cutting coefficients in the tangential and normal direction were determined from the rate of increase of cutting force as a function of chip load during separate cutting tests on a Kistler Model 9255B rigid dynamometer (see Ref. [19]). The displacement transducer output was anti-alias filtered and sampled (16-bit precision, 12,800 samples/s) with data acquisition hardware connected to a laptop computer. A periodic 1/tooth pulse was obtained with the use of a laser tachometer to sense a black–white transition on the rotating tool holder.

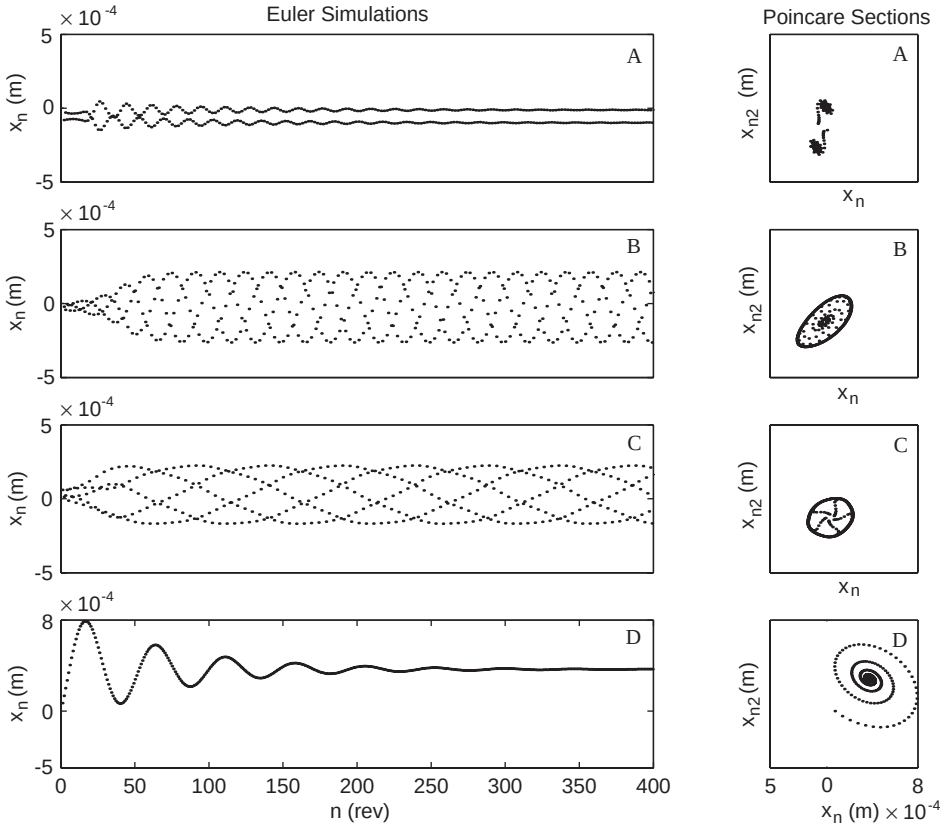

Fig. 5. Predictions of 1/tooth displacements obtained by Euler simulation for cases (A, B, C, D) of Fig. 8. Each row contains a 1/tooth displacement plot and a Poincaré section shown in delayed coordinates. Cases A ($\Omega = 3650$ r.p.m., $b = 2.3$ mm) and B ($\Omega = 3300$ r.p.m., $b = 0.8$ mm) are up-milling examples of flip and Hopf bifurcations, respectively. Cases C ($\Omega = 3600$ r.p.m., $b = 2.1$ mm) and D ($\Omega = 4350$ r.p.m., $b = 3.0$ mm) are down-milling predictions for an unstable Hopf bifurcation and a stable cutting process with substantial surface location error. Structure assumed compliant only in the x direction with dynamic and cutting coefficient parameters from Table 1. Computational time of 45 s/case using 400 steps/τ.

6.1. Bifurcation and limit cycle tests

When the flexible direction of the structure coincided with the tool feed direction, the compliant x-direction model of equation (11) was used. Aluminum (7075-T6) test specimens of width 6.35 mm and length 100 mm were mounted on the flexure and milled with a single flute 0.750-inch (19.050 mm) diameter end mill. Specimens were up-milled and down-milled at a constant feed of 0.2032 mm/rev and a fraction of the spindle period in the cut $\rho = 0.162$.

Raw displacement measurements and 1/tooth samples for the compliant x direction flexure are shown in cases (A, B, C, D) of Fig. 8. Tests were declared stable if the 1/tooth-sampled position approached a steady constant value. Unstable behavior, described as period doubling or a flip bifurcation [3,17,20], is predicted when the dominant CM of the TFEA model is negative and real with a magnitude greater than one. Experimental evidence confirms the Euler simulation and

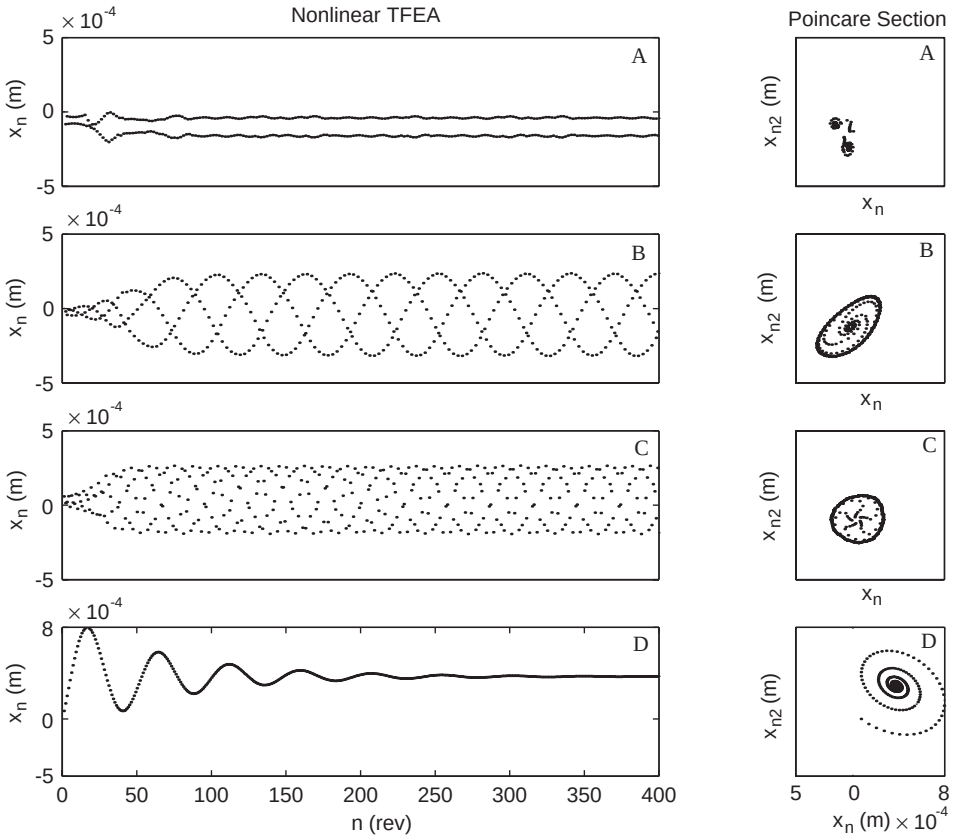

Fig. 6. Non-linear TFEA 1/tooth displacement predictions for cases (A, B, C, D) of Fig. 8. Each row contains a 1/tooth displacement plot and a Poincaré section shown in delayed coordinates. Cases A ($\Omega = 3650$ r.p.m., $b = 2.3$ mm) and B ($\Omega = 3300$ r.p.m., $b = 0.8$ mm) are up-milling examples of flip and Hopf bifurcations, respectively. Point C ($\Omega = 3600$ r.p.m., $b = 2.1$ mm) and D ($\Omega = 4350$ r.p.m., $b = 3.0$ mm) down-milling predictions for an unstable Hopf bifurcation and a stable cutting process with substantial surface location error. Structure assumed compliant only in the x direction with dynamic and cutting coefficient parameters from Table 1. Computational time of 30 s/case for unstable examples and 15 s/case for stable examples using $E = 25$.

non-linear TFEA predictions where chatter is a subharmonic of order 2 as shown in case A of Figs. 5–8. Unstable behavior predicted by complex CMs with a magnitude greater than one in the TFEA method corresponds to a Hopf bifurcation [8,16,17,24]. In such cases, chatter vibrations are unsynchronized with tooth passage as shown in examples B and C of Figs. 5–8. A stable cutting process with substantial surface location error is shown by case D. The agreement between predictions and experiment for case D of Figs. 5–8 show even a stable cutting process can have errors due to the cutting process dynamics.

6.2. *Surface location error tests*

Surface location error measurements were performed with the compliant structure direction oriented perpendicular to the tool feed. The corresponding model is given from modifying

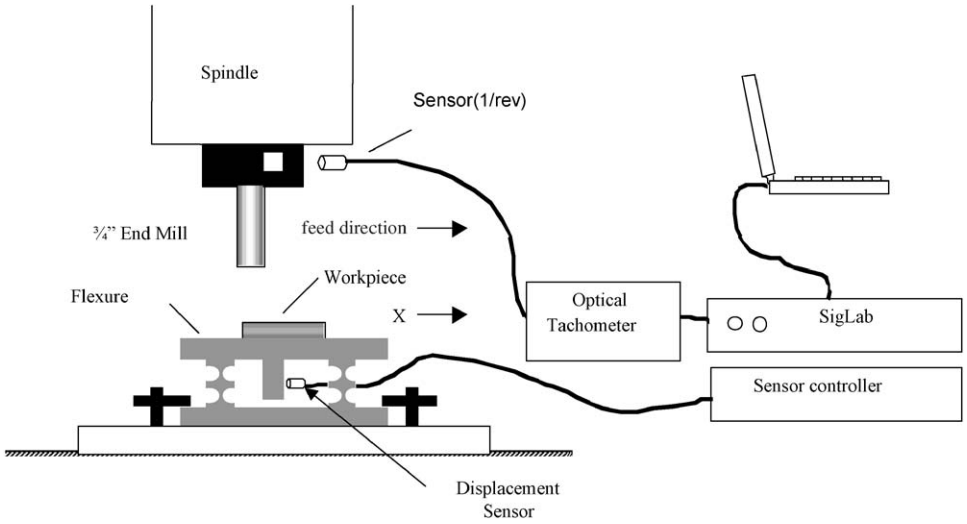

Fig. 7. Schematic of compliant x direction flexure and measurement system.

Table 1
Estimated system parameters

Symbol	x-Direction system	y-Direction system
m	2.5729 kg[a]	0.692 kg
c	5.8911 N s/m	5.7729 N s/m
k	2.18×10^6 N/m	3.01×10^6 N/m
K_t	5.5×10^8 N/m^2	5.36×10^8 N/m^2
K_n	2.0×10^8 N/m^2	1.87×10^8 N/m^2

[a] Compliant x direction flexure was mass loaded.

Eq. (10) to include only the y direction. A single flute 0.750-inch (19.050 mm) diameter end mill was used to up-mill both sides of aluminum (7050-T7451) test specimens at a fraction of the spindle period in the cut $\rho = 0.125$. Each test specimen, of length 100 mm and width 12.7 mm, was machined at a different spindle speed while holding the feed and depth of cut at constant values of $h = 0.2032$ mm/rev and $b = 1.5$ mm for all cutting tests.

Surface location error measurements were taken via two methods: (1) an eddy current displacement transducer was used along with a timing pulse from a laser tachometer, (2) a calibrated PG1000 microscope was used to visually locate the surface and the average of five measurements was used for the final result. Experimental results from each measurement method have been overlayed onto fixed point TFEA surface location error predictions in Fig. 9. The corresponding spindle speed and depth of cut points for each measurement are shown in the top stability chart. It is clearly evident that the results from each measurement technique show qualitative agreement with predictions.

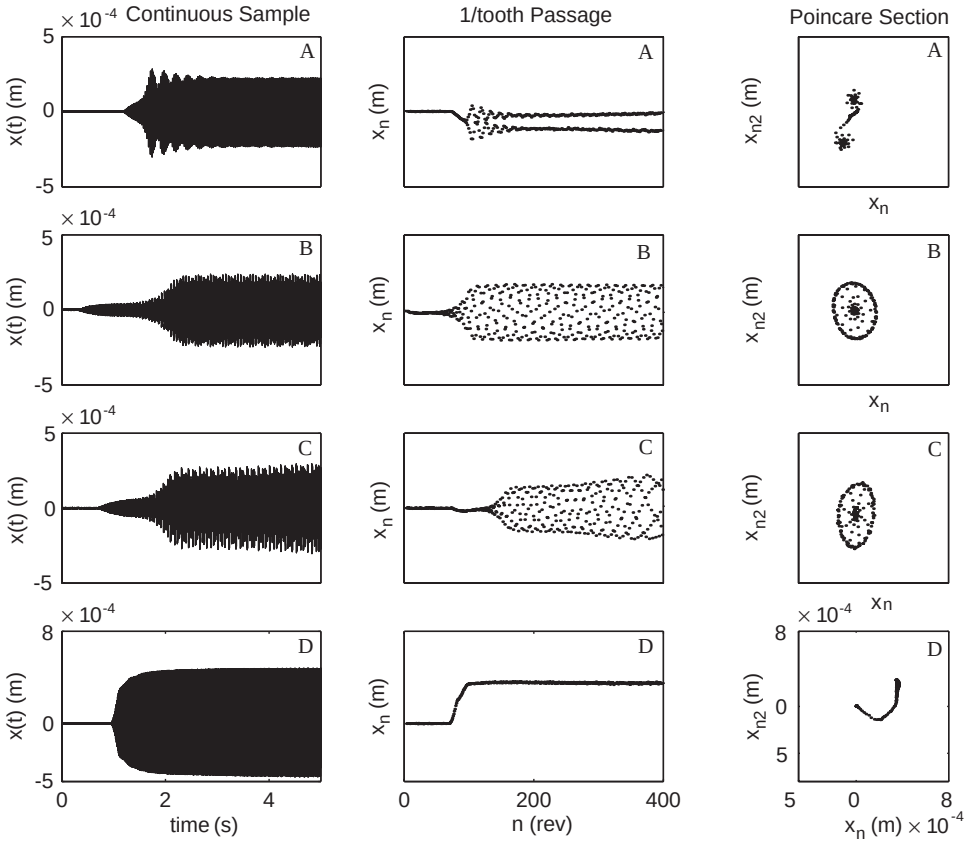

Fig. 8. Experimental measurement data for cases (A, B, C, D). Each row contains a continuous sampled displacement plot, a 1/tooth displacement plot, and a Poincaré section shown in delayed coordinates. Plots for cases A ($\Omega = 3650$ r.p.m., $b = 2.3$ mm) and B ($\Omega = 3300$ r.p.m., $b = 0.8$ mm) are unstable up-milling flip and Hopf bifurcations, respectively. Point C ($\Omega = 3600$ r.p.m., $b = 2.1$ mm) is a unstable down-milling Hopf bifurcation and point D ($\Omega = 4350$ r.p.m., $b = 3.0$ mm) is a stable down-milling process with significant surface location error.

7. Summary and conclusions

Time finite element analysis is used to analyze the accuracy, stability, and limit cycle behavior of milling. Results are compared to Euler simulation which obtains the acceleration, velocity, and displacement at each time step. Displacement information corresponding to when the cutting teeth are normal to the workpiece surface can be used to predict surface location error. Since direct stability predictions from the time-marching equations is not possible, an additional technique has been applied to quantify an unstable cutting process. Here we used the variance of simulation 1/tooth displacements to find the transition between stable and unstable cutting.

The TFEA method forms an approximate solution by dividing the time in the cut into a finite number of elements. The approximate solution is then matched with the exact solution for free vibration to obtain a discrete linear map. The formulated dynamic map is then used in three different ways: (1) stability prediction from the magnitude of map characteristic multipliers, (2)

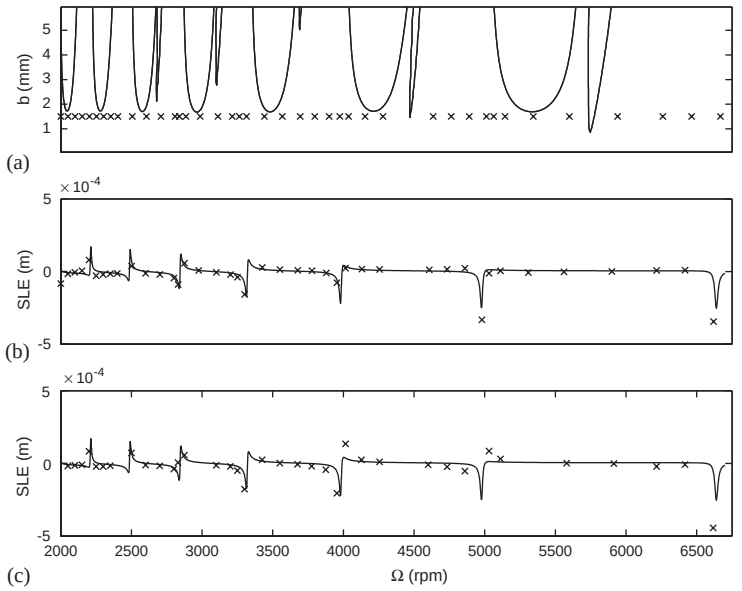

Fig. 9. Comparison between accuracy predictions and experimental values (solid line: TFEA predictions; ×: experimental values): (a) up-milling TFEA stability predictions and location of cutting tests; (b) TFEA fixed point predictions and surface location error measurements obtained from eddy current displacement transducer; and (c) TFEA fixed point predictions and surface location error measurements with PG1000 calibrated microscope. TFEA predictions assume structure is compliant only in the y direction with dynamic and cutting coefficient parameters from Table 1.

prediction of steady state surface location error from map fixed points, (3) iteration of the map to predict 1/tooth displacements for stable and unstable cutting processes. Surface location error and stability predictions are shown to be much more efficient than the Euler simulation and iteration of the map is shown to be only slightly more efficient.

TFEA surface location error, stability, and limit cycle predictions show strong agreement with both Euler simulations and experimental results. The main advantage of the TFEA method is shown to be a dramatic increase in the compuational efficiency for stability and surface location error predictions.

Acknowledgements

Support from the National Defense Science and Engineering Graduate Fellowship Program, the Boeing Company, and the NSF (DMII-9900108) is gratefully acknowledged.

References

[1] J. Tlusty, *Manufacturing Processes and Equipment*, 1st Edition, Prentice-Hall, Englewood Cliffs, Upper Saddle River, NJ, 2000.

[2] Y. Altintas, Analytical prediction of three dimensional chatter stability in milling, *JSME International Journal* 44 (3) (2001) 717–723.

[3] M.A. Davies, J.R. Pratt, B. Dutterer, T.J. Burns, Stability prediction for low radial immersion milling, *Journal of Manufacturing Science and Engineering* 124 (2) (2002) 217–225.
[4] T. Schmitz, J. Ziegert, Examination of surface location error due to phasing of cutter vibrations, *Precision Engineering* 23 (1999) 51–62.
[5] Y. Altintas, *Manufacturing Automation*, 1st Edition, Cambridge University Press, New York, NY, 2000.
[6] J. Tlusty, A. Polacek, C. Danek, J. Spacek, *Selbsterregte schwingungen an werkzeugmaschinen*, VEB Verlag Technik, Berlin, 1962.
[7] S.A. Tobias, *Machine Tool Vibration*, Blackie, London, 1965.
[8] G. Stépán, T. Kalmár-Nagy, Nonlinear regenerative machine tool vibration, *Proceedings of the 1997 ASME Design Engineering Technical Conference*, Sacramento, CA, no. DETC97/VIB-4021 (CD-ROM), p. n/a, 1997.
[9] S. Smith, J. Tlusty, An overview of the modeling and simulation of the milling process, *Journal of Engineering for Industry* 113 (1991) 169–175.
[10] Y. Altintas, E. Budak, Analytical prediction of stability lobes in milling, *CIRP Annals* 44 (1) (1995) 357–362.
[11] M.A. Davies, J.R. Pratt, B. Dutterer, T.J. Burns, Stability prediction for low radial immersion milling, *Journal of Manufacturing Science and Engineering* 124 (2) (2002) 217–225.
[12] I. Minis, R. Yanushevsky, A new theoretical approach for prediction of machine tool chatter in milling, *Journal of Engineering for Industry* 115 (1993) 1–8.
[13] T. Insperger, G. Stépán, Stability of the milling process, *Periodica Polytechnica* 44 (1) (2000) 47–57.
[14] T. Insperger, G. Stépán, Stability of high-speed milling, *Proceedings of Symposium of Nonlinear Dynamics and Stochastic Mechanics*, no. AMD-241, Orlando, FL, 2000, pp. 119–123.
[15] W.T. Corpus, W.J. Endres, A high order solution for the added stability lobes in intermittent machining, *Proceeding of the Symposium on Machining Processes*, no. MED-11, 2000, pp. 871–878.
[16] P.V. Bayly, J.E. Halley, B.P. Mann, M.A. Davies, Stability of interrupted cutting by temporal finite element analysis, September 2001.
[17] B.P. Mann, T. Insperger, P.V. Bayly, G. Stépán, Stability of up-milling and down-milling, Part 2: experimental verification, *International Journal of Machine Tools and Manufacture* 43 (2003) 35–40.
[18] L. Meirovitch, *Elements of Vibration Analysis*, 2nd Edition, McGraw-Hill, New York, 1986.
[19] J.E. Halley, Stability of Low Radial Immersion Milling, Master's Thesis, Washington University, Saint Louis, 1999.
[20] P.V. Bayly, B.P. Mann, M.A. Davies, J.R. Pratt, Stability analysis of interrupted cutting with finite time in the cut, *Proceedings of ASME Design Engineering Technical Conference, Manufacturing in Engineering Division*, Orlando, FL, MED-11 (2000) 989–994.
[21] P.V. Bayly, B.P. Mann, T.L. Schmitz, D.A. Peters, G. Stépán, T. Insperger, Effects of radial immersion and cutting direction on chatter instability in endmilling, *Proceedings of ASME International Mechanical Engineering Conference and Exposition, New Orleans, LA*, no. IMECE2002-34116, New Orleans, LA, ASME, 2002.
[22] D.A. Peters, A.P. Idzapanah, Hp-version finite elements for the space–time domain, *Computational Mechanics* 3 (1988) 73–78.
[23] Y. Jaluria, *Computational Heat Transfer*, 1st Edition, Hemisphere Publishing Corporation, Washington, 1986.
[24] L.N. Virgin, *Introduction to Experimental Nonlinear Dynamics*, Cambridge University Press, Cambridge, UK, 2000.
[25] L.J. Hou, D.A. Peters, Application of triangular space–time finite elements to problems of wave propagation, *Journal of Sound and Vibration* 173 (5) (1994) 611–632.
[26] D. Montgomery, Y. Altintas, Mechanism of cutting force and surface generation in 20 dynamic milling, *Journal of Engineering for Industry* 113 (1991) 160–168.
[27] J. Tlusty, F. Ismail, Basic non-linearity in machining chatter, *Annals of the CIRP* 30 (1981) 21–25.
[28] T.L. Schmitz, Chatter recognition by a statistical evaluation of the synchronously sampled audio signal, *Proceedings of the 2001 India–USA Symposium on Emerging Trends in Vibration and Noise Engineering*, Columbus, OH, December 10–14, 2001.
[29] T.L. Schmitz, K. Medicus, B. Dutterer, Exploring once-per-revolution audio signal variance as a chatter indicator, *Machining Science and Technology* 6 (2) (2002) 215–233.
[30] S.H. Strogatz, *Nonlinear Dynamics and Chaos*, 1st Edition, Perseus Books, Reading, MA, 1994.
[31] E. Kreyszig, *Advanced Engineering Mathematics*, 8th Edition, Wiley, New York, NY, 1999.
[32] D.J. Inman, *Engineering Vibration*, 2nd Edition, Prentice-Hall, Upper Saddle River, NJ, 2001.